AGU PUBLICATIONS

Geophysical Research Letters

RESEARCH LETTER
10.1002/2016GL069553

Special Section:
First results from NASA's Magnetospheric Multiscale (MMS) Mission

Estimates of terms in Ohm's law during an encounter with an electron diffusion region

R. B. Torbert[1,2], J. L. Burch[2], B. L. Giles[3], D. Gershman[3], C. J. Pollock[3], J. Dorelli[3], L. Avanov[3], M. R. Argall[1], J. Shuster[1], R. J. Strangeway[4], C. T. Russell[4], R. E. Ergun[5], F. D. Wilder[5], K. Goodrich[5], H. A. Faith[1], C. J. Farrugia[1], P.-A. Lindqvist[6], T. Phan[7], Y. Khotyaintsev[8], T. E. Moore[3], G. Marklund[6], W. Daughton[9], W. Magnes[10], C. A. Kletzing[11], and S. Bounds[11]

[1]Physics Department and Space Science Center, University of New Hampshire, Durham, New Hampshire, USA, [2]Southwest Research Institute, San Antonio, Texas, USA, [3]NASA Goddard Space Flight Center, Greenbelt, Maryland, USA, [4]Department of Earth, Planetary, and Space Sciences, University of California, Los Angeles, California, USA, [5]Laboratory of Atmospheric and Space Physics, University of Colorado, Boulder, Colorado, USA, [6]Royal Institute of Technology, Stockholm, Sweden, [7]Space Science Center, University of California, Berkeley, California, USA, [8]Swedish Institute of Space Physics, Uppsala, Sweden, [9]Los Alamos National Laboratory, Los Alamos, New Mexico, USA, [10]Space Research Institute, Austrian Academy of Sciences, Graz, Austria, [11]Department of Physics, University of Iowa, Iowa City, Iowa, USA

Key Points:
- Pressure Gradient and Inertial Terms in Ohm's law evaluated in an Electron Diffusion Region
- Ion and electron Frozen-in Condition observed to be broken

Supporting Information:
- Supporting Information S1

Correspondence to:
R. B. Torbert,
roy.torbert@unh.edu

Citation:
Torbert, R. B., et al. (2016), Estimates of terms in Ohm's law during an encounter with an electron diffusion region, *Geophys. Res. Lett.*, *43*, 5918–5925, doi:10.1002/2016GL069553.

Received 11 MAY 2016
Accepted 26 MAY 2016
Accepted article online 28 MAY 2016
Published online 16 JUN 2016

Abstract We present measurements from the Magnetospheric Multiscale (MMS) mission taken during a reconnection event on the dayside magnetopause which includes a passage through an electron diffusion region (EDR). The four MMS satellites were separated by about 10 km such that estimates of gradients and divergences allow a reasonable estimate of terms in the generalized Ohm's law, which is key to investigating the energy dissipation during reconnection. The strength and character of dissipation mechanisms determines how magnetic energy is released. We show that both electron pressure gradients and electron inertial effects are important, but not the only participants in reconnection near EDRs, since there are residuals of a few mV/m (~30–50%) of $\mathbf{E}+\mathbf{U}_e\times\mathbf{B}$ (from the sum of these two terms) during the encounters. These results are compared to a simulation, which exhibits many of the observed features, but where relatively little residual is present.

1. Introduction

The pervasive magnetic field in space is responsible for many of the energetic phenomena in our plasma universe. Over past decades, it has become increasingly clear that magnetic reconnection, as originally suggested by several authors [*Dungey*, 1953, 1961; *Cowling*, 1953], is a universal process that converts magnetic field energy, often explosively, to rapid flow jets and very energetic particle fluxes associated with episodic events, such as solar flares and mass ejections, geomagnetic storms, aurora, and astrophysical cousins such as radio jets. The study of the energy dissipation mechanisms in reconnection is critical to understanding the time scale of this energy release, as first elucidated by Sweet and Parker [*Parker*, 1957] and is a prime objective of the Magnetospheric Multiscale (MMS) mission [*Burch et al.*, 2015]. A key part of this study is the evaluation of the relative contributions of various terms in the generalized Ohm's law which relates electric field and currents and how each of these terms contributes to energy conversion. In the form emphasizing the electron contributions and valid for $m_e << m_i$, this is [*Gurnett and Bhattacharjee*, 2005]

$$\mathbf{E}+\mathbf{U}_e\times\mathbf{B}=\eta\mathbf{J}-\frac{1}{en}\nabla\cdot\overleftrightarrow{\mathbf{P}}_e+\frac{m_e}{en}\left(\frac{\partial\mathbf{J}}{e\partial t}+\nabla\cdot n(\mathbf{U}_i\mathbf{U}_i-\mathbf{U}_e\mathbf{U}_e)\right) \quad (1)$$

where $\mathbf{U}_e$ and $\mathbf{U}_i$ are the electron and ion bulk velocities, $\mathbf{P}_e$ is the full electron pressure tensor, $\mathbf{E}$, $\mathbf{B}$, and $\mathbf{J}$ are the usual electric, magnetic, and current field vectors, and η is the remaining resistivity that may be due to collisions (usually negligible), wave-particle interactions, or unaccounted kinetic effects. (Not explicitly evaluated here, the term $\eta\mathbf{J}$, which we call the "residue," is best thought to represent what we do *not* yet know in Ohm's law.) The so-called "frozen-in" condition applies when the curl of the left-hand side of this equation is zero; thus, determining that $\mathbf{E}'\equiv\mathbf{E}+\mathbf{U}_e\times\mathbf{B}=0$ is sufficient to satisfy this condition. The evaluation of these quantities has been attempted previously in the Cluster mission [*Andre et al.*, 2004; *Khotyaintsev et al.*, 2006], but the time resolution of the data and larger spacecraft separation could not support the complete investigation of equation (1) at the electron scale. The four MMS satellites [*Burch et al.*, 2015; *Torbert et al.*, 2014] are instrumented

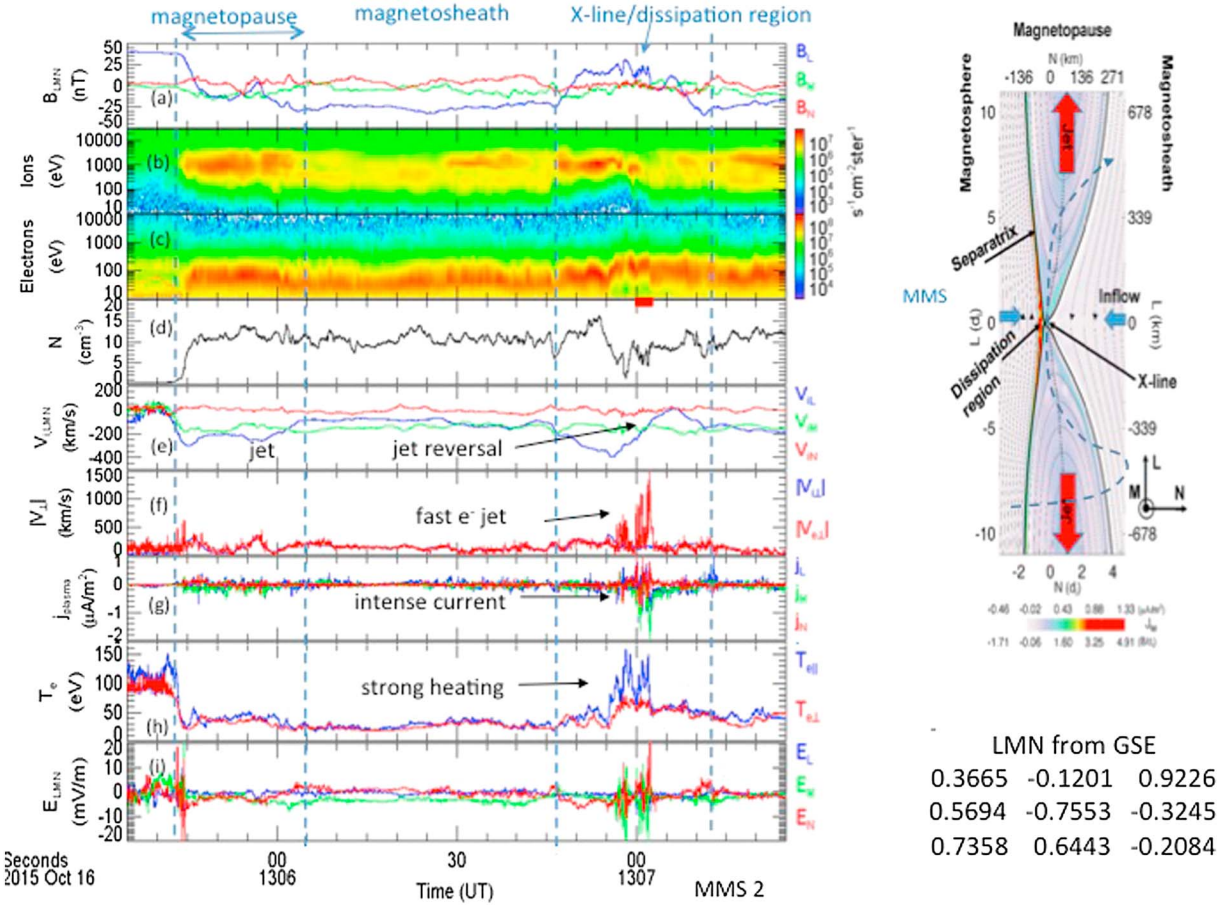

Figure 1. Parameters of the magnetopause crossing: (a) **B**, (b, c) the ion and electron omnidirectional spectrograms, (d) ion density, (e) ion velocity, (f) electron perpendicular velocity, (g) current, (h) electron temperature, and (i) **E**. Right: schematic of MMS path through EDR (With permission, *Science*).

specifically to provide the capability to estimate these terms and how they contribute to the frame invariant quantity that measures the rate of conversion of magnetic energy: $\mathbf{J}\cdot\mathbf{E}'$. Although the careful cross calibration of all sensors contributing to equation (1) will surely continue to be improved throughout the entire MMS mission, this letter presents our first attempt to make these estimates with the best calibrations available now. The importance of this subject to reconnection studies, and to the question of the time scale for energy release, argues for reporting what we do know at the present time. This communication will focus on one event where, as reported in [*Burch et al.*, 2016], the MMS constellation very clearly encountered an active electron diffusion region (EDR). The reader is referred to that paper for additional background information.

2. Observations

The four MMS satellites encountered the magnetopause current layer three times in the dusk sector between 13:05:25 and 13:07:25 on 16 October 2015, as seen in Figure 1, which is reproduced in part from Figure 3 of *Burch et al.* [2016]. These data are from the MMS2 satellite, but on this scale, the data from all four satellites look very similar. MMS exited the magnetosphere (MSP) first at 13:05:42, partially re-entered at 13:06:46, and finally exited near 13:07:10, as seen in the B_L component, the ion and electron omnidirectional spectrograms, and the ion density. The *LMN* coordinate system was determined from a minimum variance magnetic field analysis done on the complete crossing between 13:05:40 and 13:06:09. Although only a southward ion jet was seen in the first crossing, a reversal in ion flow is very prominent in the encounters between 13:06:46 and 13:07:10. The distinct fast electron jet, the intense currents (strongest duskward), and the strong electron heating, along with an in-depth analysis of the electron distribution functions, led *Burch et al.* [2016] to conclude that the MMS fleet traversed an EDR around 13:07:02 (red bar in Figure 1d), as diagrammed in the

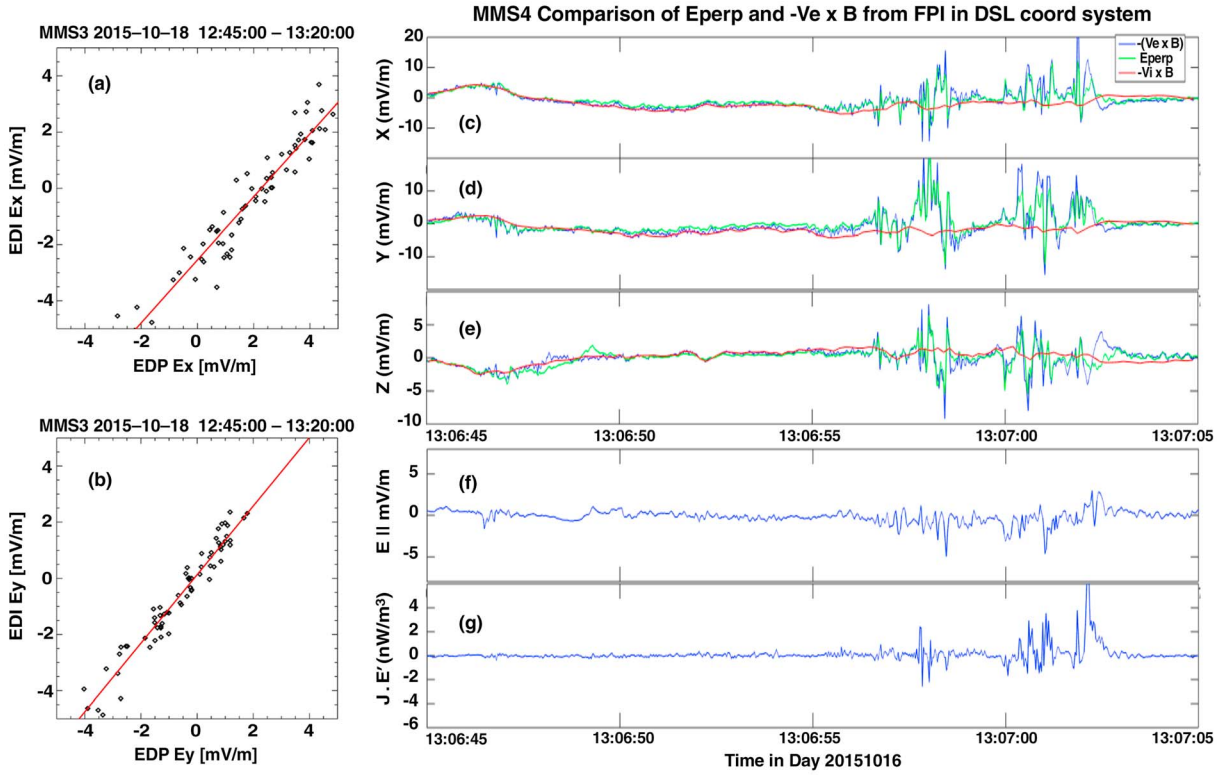

Figure 2. (a and b) Comparison of EDI electric fields to those of EDP and the three components of (c–e) $\mathbf{E}_{perp}$, $-\mathbf{U}_e \times \mathbf{B}$, and $-\mathbf{U}_i \times \mathbf{B}$, as well as (f) the parallel *E* component and (g) the total power dissipation ($\mathbf{J} \cdot \mathbf{E}'$) for the MMS4 spacecraft in Sun-aligned (with *z* along spin axis) coordinates (DSL).

simulation graphic seen in Figure 1. In view of the brevity of the reversed $\mathbf{U}_i$ flow, the encounter with northern exhaust may have been brief, but that is not important to these results. Rather, this letter will analyze the contributions to Ohm's law in the EDR interval between 13:06:59 and 13:07:04.

A major component of the mission design was the accurate calibration, both before and after launch, of the sensors that contribute to the determination of the terms in equation (1). In particular, the electromagnetic fields [*Torbert et al.*, 2014] and particle velocities, as determined by the Fast Plasma Instrument [*Pollock et al.*, 2016], must be cross calibrated to within 1–2 mV/m for each term. The electric field sensors (Spin-plane Double Probe (SDP) [*Lindqvist et al.*, 2014] and Axial Double Probes (ADP) [*Ergun et al.*, 2014]) have been checked against the Electron Drift Instrument (EDI) [*Torbert et al.*, 2015] to reduce systematic errors. Figures 2a and 2b show the cross calibration of the spin-plane *x* and *y* components, for example, of the SDP with that of EDI. The slight variation of the slope from a value of 1 is used to adjust the shorting factors [*Fahleson*, 1967] of the double probe for these measurements and to determine the offsets due to spacecraft perturbations. In addition, in the magnetosheath (MSH) regions, such as 13:06:10 to 13:06:46 in Figure 1, where the right-hand side of equation (1) should be near zero, the EDP data can be checked against both $-\mathbf{U}_e \times \mathbf{B}$ and $-\mathbf{U}_i \times \mathbf{B}$. The results seen in Figures 2c–2e show that MMS has achieved cross calibration to within 1 mV/m.

It is important to note when $\mathbf{E} + \mathbf{U}_{(e,i)} \times \mathbf{B}$ is significantly different from zero. Figures 2c–2e also show that when MMS4 (other spacecraft are similar) passes back and forth near separatrices, between 13:06:47 and 13:07:03 (see trajectory in Figure 1), the three disagree by much more than 1 mV/m. Note that the time resolution for the moments (ions, 150 ms; electrons, 30 ms) is adequate to determine the frozen-in condition for both species. In particular, as the ions are more massive, they do not follow the $\mathbf{E} \times \mathbf{B}$ velocity as MMS crosses the current sheets, but the lighter electrons do, except in the EDR near 13:07:02.4 for this spacecraft. Although at this stage of calibration, the error $\mathbf{E}\|$ is ~2 mV/m, distinct spikes (at 13:06:58.5 and 13:07.01) of higher magnitude are seen to occur throughout the separatrix encounters, as is seen in many simulations [e.g., *Pritchett and Mozer*, 2009]. The presence of nearly 6 nW/m^{-3} of power per unit volume dissipated in the electron rest

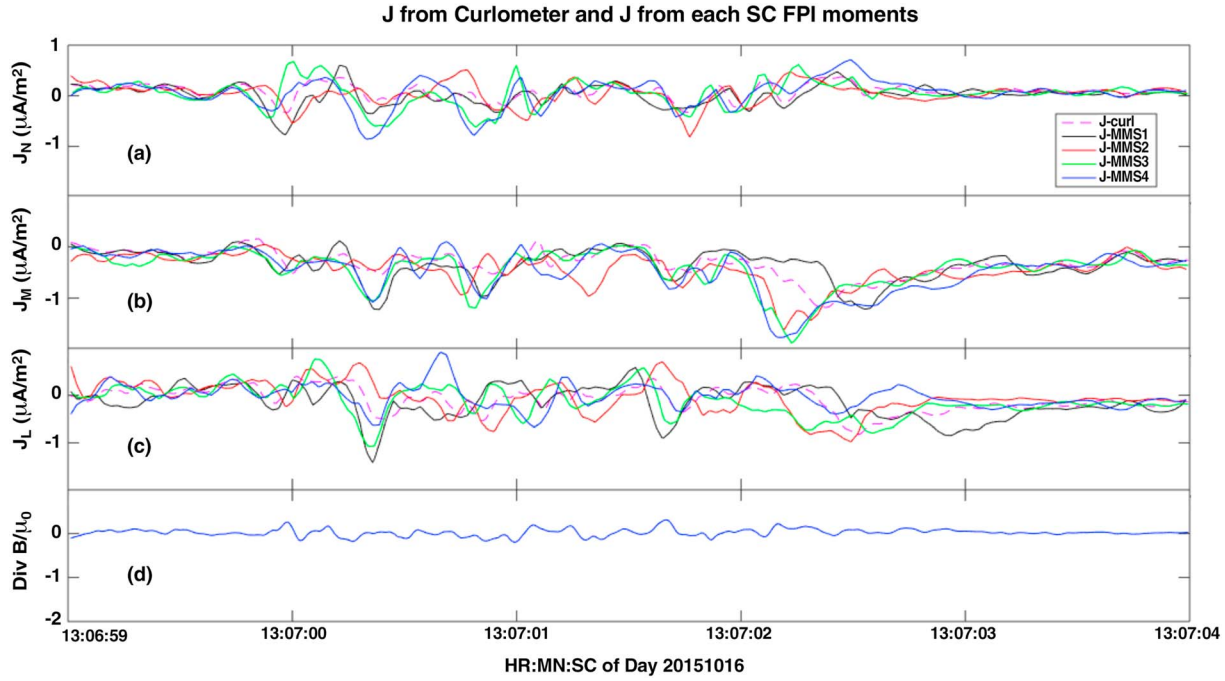

Figure 3. (c, b, and a) The *LMN* components of current from the individual spacecraft and from the curlometer, as well as (d) $\nabla \cdot B/\mu_0$.

frame (Figure 2g, $\mathbf{J} \cdot \mathbf{E}'$) has been shown by other simulations [*Zenitani et al.*, 2011] to be a strong indicator of proximity to the EDR, even though regions surrounding it may have fluctuations to small negative values, which have been seen also in simulations [*Zenitani et al.*, 2011; *Pritchett and Mozer*, 2009].

In this high-density region ($n \sim 5$–$10\ \mathrm{cm}^{-3}$), the Poisson statistical errors in the velocities are negligible. Given that the errors are thus primarily systematic and apparently $<$ ~1 mV/m, these data make clear that there is an extensive region where the ions are not frozen in and a much smaller, more compact region where the electrons are not frozen in (EDR) and where measurable energy dissipation is occurring.

3. Gradient and Divergence Computations

MMS separation strategy was designed to allow a calculation of gradient, divergence, and curl of tensor fields [*Paschmann and Daly*, 1998]. There are three major sources of error in this endeavor. The first is the error in the relative positions of the satellites. MMS was designed with a state-of-the-art GPS system that determines absolute positions to within a few meters [*Tooley et al.*, 2015], and thus, for separations of even 10 km, the contribution from this source is negligible. Second, since the statistical errors are small, as said above, the systematic errors in the quantities themselves are more important. MMS runs and will continue to run throughout the entire mission, an intensive calibration and cross-calibration program, and will undoubtedly improve the accuracy of relevant parameters, but the best presently calibrated data above have shown that for terms in equation (1), an error of ~$<$1 mV/m is achieved. Third, the gradients determined from reciprocal vectors make sense only if the spacecraft are within a structure where linear approximations are reasonable. The separation of 10 km (about 4–6 electron inertial lengths, $d_e = 1.6$–2.3 km, for this crossing) is the closest possible at present with MMS and may be a reasonable compromise between systematic errors resulting from small differences versus those resulting from separations that are too far. Moreover, this third error can be assessed by examining the profiles of the currents computed from individual spacecraft ($en(\mathbf{U}_i - \mathbf{U}_e)$) and comparing these to the current profile determined from the curlometer technique [*Dunlop et al.*, 1988]. Figures 3a–3c show this comparison for 5 s around the EDR. It is apparent particularly that the $\mathbf{J}_M$ components are very similar in profile and magnitude if time shifted to account for spacecraft position (MMS1 lags during this inward motion of the boundary), although both other components also show correlation to some degree. The normal velocity deduced from the relative timing of the currents is about 35–45 km/s. Thus, the width of the current layer is about 12–15 km, greater than the normal separation of the spacecraft at this

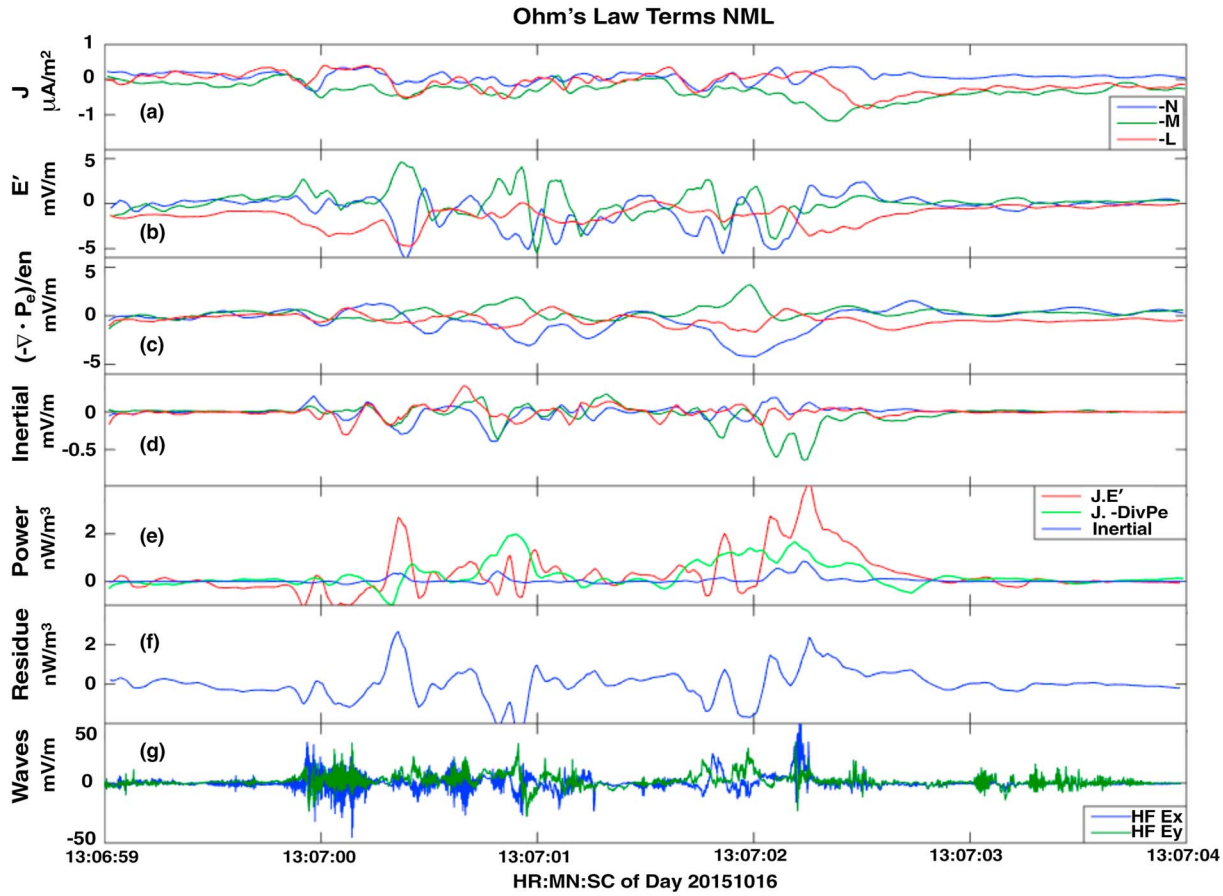

Figure 4. (b–d) The comparison of terms in Ohm's law for interval around 13:07:02 and (e) the total power dissipation from individual terms. (f) The residue, $\mathbf{J}\cdot(\mathbf{E}' - (-\nabla\cdot P_e)/en_e - m_e[\nabla\cdot(n_e(\mathbf{U}_i\mathbf{U}_i - \mathbf{U}_e\mathbf{U}_e)]/en_e)$.

time [see *Burch et al.*, 2016, Figure 1b]. It is also worth noting that although the width of the current layer is about 6–8 d_e, the width of the $\mathbf{J}\cdot\mathbf{E}'$ (Figure 2g) dissipation layer is about one third the size. Finally, Figure 3d shows the computation of $\nabla\cdot\mathbf{B}/\mu_0$ ($\mu A/m^2$). Since this value deviates from $\nabla\times\mathbf{B}/\mu_0$ by less than 10%, we conclude that the divergence computations are for data taken within a reasonably uniform layer.

The fluid description of dissipation in the EDR is described by Ohm's law. Figure 4 shows the first attempt using MMS data to compare the various terms contributing to this dissipation. Figure 4a shows again the three components of the magnetopause current determined from the curlometer method. The *M* component of the current peaks at about 13:07:02.3 which is near the average (over four spacecraft) encounter time of the EDR. Figure 4b is $\mathbf{E}'$ (left-hand side of equation (1)), computed from the average of that quantity determined by the electron and ion moments for all four spacecraft (whereas Figure 2 was for MMS4 only), showing again the same nonzero interval, when electrons are likely not frozen in. Technically, such "nonfrozen-in flow" occurs when the curl of this quantity is nonzero, but in practice, that is probable whenever there is significant deviation of $\mathbf{E}'$ from zero, as is the case from 13:06:59.8 to about 13:07:02.75, during which the MMS constellation skirted along the separatrix and traversed the EDR. Note that outside these times, the *average* $\mathbf{E}'$ (again, Figure 2 is for one spacecraft) also is within 0.5 mV/m of zero, except for the *L* component. This component derives mostly from the axial antennae on MMS, which are the most prone to errors from spacecraft perturbations [*Ergun et al.*, 2014], but even that component is zero to within ~1.5 mV/m. We conclude that for the *N* and *M* components, these data show that the systematic errors are about 0.5 mV/m and a little worse on the *L* component. Of similar magnitude to $\mathbf{E}'$ is the gradient of the electron pressure term in Figure 4c. The form of this quantity is different from that of Figure 4b, implying that the dynamical contributions are varying throughout this interval with spatial or temporal structure, but the distinct negative excursion at 13:07:02.0 and then the reversal to positive at 13:07:02.3 in the normal component in both Figures 4b

and 4c suggest that the pressure gradient supports the normal component of the electric field, as is seen in other reported data [*Argall*, 2014] in *Mozer and Pritchett* [2009] and below in our analysis of simulations by *Daughton et al*. [2014].

The inertia term is evaluated in Figure 4d by computing $(m_e/en)\cdot\nabla\cdot(n(\mathbf{U}_i\mathbf{U}_i-\mathbf{U}_e\mathbf{U}_e))$ in the moving frame of the boundary (supporting information Text S1). In that frame, the contributions from $\partial\mathbf{J}/\partial t$ should be small. This assumption can be checked with the data in Figure 3 by noting that the peak in the largest **J** component, *M*, for MMS1 lags those of the other spacecraft by about 0.3 s, because MMS1 is the last to go through the layer. If the difference in peak current (~0.7 $\mu A/m^2$) is all due to time variation, the maximum contribution of this term is about 0.02 mV/m, negligible compared to those plotted in Figure 4d. It is seen that the contributions of the inertial term (due to changing flows of the electrons) are generally smaller than the overall values of **E′** and the pressure term. However, if one concentrates on the *M* (green) component only, which is primarily along the reconnection electric field, then the distinct negative excursion to −0.6 mV/m between 2.0 and 2.3 s is comparable to the pressure term at that time and is occasionally 15–60% of $\mathbf{E}'_M$, although, as stated above, our error in **E′** itself is about 0.5 mV/m. This negative peak is the fluid signature of the "crescent" feature seen in the individual electron velocity distributions, as reported in *Burch et al*. [2016], and reflects the turning of electrons at the current boundary from inward flow to flow along the magnetopause.

After taking into account the pressure gradient and the inertial terms, the residual remains significant. To illustrate this result, we have plotted in Figure 4e the total power in each of three terms: **J** dotted into each of **E′** (red), the pressure term (green), and the inertial term (blue). The difference of the first from the sum of the other two, the residual, is plotted in Figure 4f. The pressure term accounts for a significant fraction (occasionally up to 80%) of the power, and the inertial term makes a contribution right at the EDR. However, the residual is of the same order as the total $\mathbf{J}\cdot\mathbf{E}'$. To test whether there is any crude correlation with wave turbulence, Figure 4g shows the full wave amplitude at frequencies up to 4 kHz (including modes such as whistler and hybrid drift waves). The wave power is much more spatially localized than anticipated (the burst at 13:07:02.2 is only 1–2 d_e in size) and has no obvious correlation with the residual, except at the EDR itself, where the power is greatest and may account for the sharp peak in $\mathbf{J}\cdot\mathbf{E}'$. The proper determination of the contribution of waves requires a detailed mode analysis, which is underway within the MMS team.

4. Comparison to Simulations

The data in Figure 4 undoubtedly depend on the actual path of MMS through the magnetopause structures surrounding the EDR. In this section, we compare the predictions of a particle-in-cell simulation of these parameters to those of the MMS observations, keeping in mind the inferred trajectory given in Figure 1. The 2.5-D simulation in Figure 5 models asymmetric reconnection, with zero guide field (applicable to this event [*Burch et al*., 2016]). Details that are described in the supporting information Text S2 show that $v_{Ai}\cdot B_0\sim 5$ mV/m; thus, the magnitudes in Figures 5a–5c correspond to ~10 mV/m, the *M* components, Figures 5d–5i, are ~1–2 mV/m, and the power, Figures 5j–5l, ~1 nW/m^3.

Figure 5 shows the relative magnitudes and *M* (out of plane) components of three terms of the generalized Ohm's law: the electric field in the electron rest frame, **E′**, the divergence of the electron pressure tensor $(-\nabla\cdot P_e)/en_e$, and the electron inertia term, neglecting temporal derivatives, $m_e[-\nabla\cdot(n_e\mathbf{U}_e\mathbf{U}_e)]/en_e$ (the $\mathbf{U}_i\mathbf{U}_i$ term is ignored because both simulation and data in Figure 2 show that it is sufficiently uniform over these spatial scales).

The simulation values have been smoothed over a spatial scale of 3.9 d_e to approximate that of the data. The structure in Figures 5a and 5b is due to the strong in-plane Hall electric field $\mathbf{E}'_N$ mainly balanced by $\partial_N(P_{e,NN})/en_e$ (since $P_{e,NN}>>P_{e,LN}$), which result in magnitudes of this term about an order of magnitude larger than $|m_e[-\nabla\cdot(n_e\mathbf{U}_e\mathbf{U}_e)]/en_e|$ and the *M* components of each term. This balance in the data for $\mathbf{E}'_N$ at 13:07:02 (Figures 4b and 4c), near the EDR, has been noted above.

On the low-density MSP side of the layer (on the left, $N<0$), the *M* component of $\mathbf{E}'_M$ (Figure 5d) is mainly balanced by the $\partial_N(P_{e,MN})/en_e$ part of the *M* component $(-\nabla\cdot P_e)_M/en_e$ (Figure 5e), and the inertial term, $m_e[-\nabla\cdot(n_e\mathbf{U}_e\mathbf{U}_e)]_M/en_e$ (Figure 5f), is small. On the MSH side, the inertial term $m_e[\nabla\cdot(n_e\mathbf{U}_e\mathbf{U}_e)]_M/en_e$ together with $\mathbf{E}'_M$ helps to balance $(\nabla\cdot P_e)_M/en_e$. An examination of the spatial character of the *M* components in Figures 5d–5f shows that although these values depend highly on both the *L* and *N* location, with a large

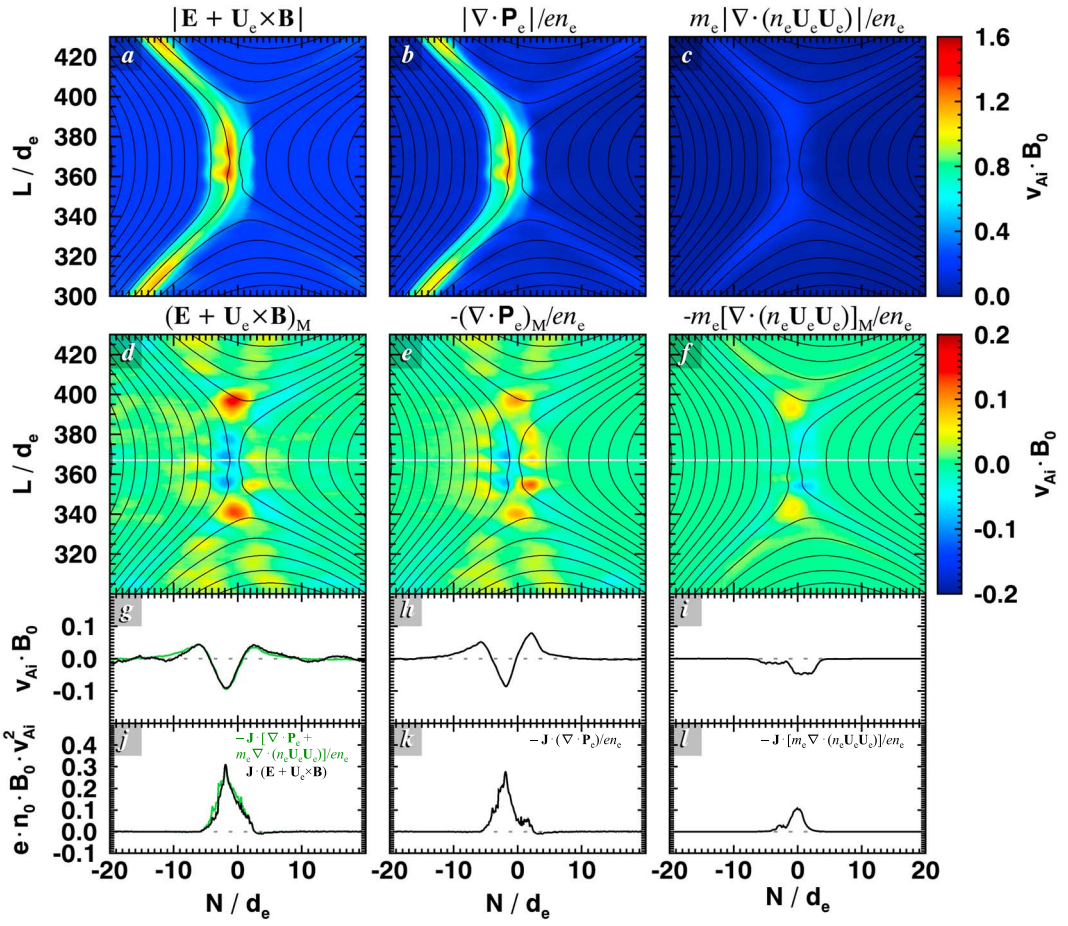

Figure 5. Structure of the electron diffusion region (EDR) in three terms of the electron momentum equation from a PIC simulation of asymmetric reconnection: (a–c) magnitudes and (d–f) *M* components **E′**, the divergence of the electron pressure tensor $(-\nabla \cdot P_e)/en_e$, and the inertia term $m_e[-\nabla \cdot (n_e\mathbf{U}_e\mathbf{U}_e)]/en_e$. (g–i) Cuts through the EDR of the *M* components and (j–l) power along $x/d_e = 367$ (white lines). The green curves in Figures 5g and 5j are the sums of pressure and inertia terms. Normal simulation *x* coordinate (vertical) has been mapped to data *L*, whereas *z* (horizontal) is data $-N$.

amount of structure, there is generally a smaller value of the inertial term on the MSP side. Thus, these simulation results might suggest that the path of MMS skirted the MSP side of the layer.

The overall magnitudes, the balance in the normal component, and the distinct feature in the inertial term are thus all reflected in the observations. For the simulation, the sums of the *M* components (and power, $\mathbf{J} \cdot []$) of the gradient $\mathbf{P}_e$ and inertial terms is plotted as the green trace in Figures 5g (and 5j). These traces show overall balance with **E′** (and $\mathbf{J} \cdot \mathbf{E}'$). We have performed this comparison by smoothing the simulation data over a scale up to 6.3 d_e, and whereas the actual values are naturally reduced by up to a factor of 2, the balance of the terms remains. This is quite in contrast to the large residual for the data seen in Figure 4f. This balance should not be affected by the actual path of the satellites near the EDR and thus may reflect a different set of mechanisms than is represented in only the pressure and inertial terms of the fluid Ohm's law.

5. Conclusions

These observations demonstrate that MMS is making progress in the quantitative evaluation of important terms in Ohm's law. The average value of the peak dissipation, $\mathbf{J} \cdot \mathbf{E}' \sim 4\ \mathrm{nW/m^3}$, supports the conclusion that fast reconnection is occurring near EDRs. There are significant contributions to the dynamics from the $\nabla \cdot P_e$ term, overall, and in the *M* component, from both the $\nabla \cdot P_e$ and inertial terms. However, values of the residual imply that the pressure and inertial terms may not be sufficient to close Ohm's law, in contrast to what is seen in 2-D simulations. Three-dimensional simulations show enhanced fluctuations, not seen in 2-D [*Daughton*

et al., 2011], which in collisionless plasmas contributes to the only remaining term, $\eta\mathbf{J}$, through anomalous transport. The large value of the unidentified residual (up to 50% of the total) implies that such fluctuations may play an important role at the EDR. A more complete understanding of the relative contributions of these terms may come from improved calibration of data, closer relative spacecraft separations (being planned for MMS), or analyses of the contributions of turbulence in both the wave data and 3-D simulation. The enhanced capabilities of MMS will allow us to pursue these studies and lead to a more accurate picture of reconnection.

Acknowledgments
We thank the successful MMS team for such wonderful data (available at https://lasp.colorado.edu/mms/sdc/public/) and NASA support via contract NNG04EB99C.

References

Andre, M., A. Vaivads, S. C. Buchert, A. N. Fazakerley, and A. Lahiff (2004), Thin electron-scale layers at the magnetopause, *Geophys. Res. Lett*, *31*, L03803, doi:10.1029/2003GL018137.

Argall, M. R. (2014), Estimating proximity to the asymmetric reconnection X-line, PhD thesis, University of New Hampshire.

Burch, J. L., T. E. Moore, R. B. Torbert, and B. L. Giles (2015), Magnetospheric Multiscale overview and science objectives, *Space Sci. Rev.*, doi:10.1007/s11214-015-0164-9.

Burch, J. L., et al. (2016), Electron-scale measurements of magnetic reconnection in space, *Science*, in press, doi:10.1126/science.aaf2939.

Cowling, T. G. (1953), Solar electrodynamics, in *The Sun*, edited by G. P. Kuiper, pp. 532–591, Univ. of Chicago Press, Chicago.

Daughton, W., V. Roytershteyn, H. Karimabadi, L. Yin, B. J. Albright, B. Bergen, and K. J. Bowers (2011), Role of electron physics in the development of turbulent magnetic reconnection in collisionless plasmas, *Nat. Phys.*, *7*(7), 539–542, doi:10.1038/nphys1965.

Daughton, W., T. K. M. Nakamura, H. Karimabadi, V. Roytershteyn, and B. Loring (2014), Computing the reconnection rate in turbulent kinetic layers by using electron mixing to identify topology, *Phys. Plasmas*, *21*, 052307, doi:10.1063/1.4875730.

Dungey, J. W. (1953), Conditions for the occurrence of electrical discharges in astrophysical systems, *Philos. Mag.*, *44*, 725–739.

Dungey, J. W. (1961), Interplanetary magnetic field and the auroral zones, *Phys. Rev. Lett.*, *6*, 47–48.

Dunlop, M. W., D. J. Southwood, K.-H. Glassmeier, and F. M. Neubauer (1988), Analysis of multipoint magnetometer data, *Adv. Space Res.*, *8*(9–10), 273–277, doi:10.1016/0273-1177(88)90141-X.

Ergun, R. E., et al. (2014), The axial double probe and fields signal processing for the MMS mission, *Space Sci. Rev.*, 1–22, doi:10.1007/s11214-014-0115-x.

Fahleson, U. (1967), Theory of electric field measurements conducted in the magnetosphere with electric probes, *Space Sci. Rev.*, *7*, 238–262.

Gurnett, D., and A. Bhattacharjee (2005), *Introduction to Plasma Physics*, p. 179 (Eq. 6.1.17), Cambridge Univ. Press, Cambridge, U. K.

Khotyaintsev, Y. V., A. Vaivads, A. Retino, M. Andre, C. J. Owen, and H. Nilsson (2006), Formation of inner structure of a reconnection separatrix region, *Phys. Rev. Lett.*, *97*, 205003.

Lindqvist, P.-A., et al. (2014), The spin-plane double probe electric field instrument for MMS, *Space Sci. Rev.*, 1–29, doi:10.1007/s11214-014-0116-9.

Mozer, F. S., and P. L. Pritchett (2009), Regions associated with electron physics in asymmetric magnetic field reconnection, *Geophys. Res. Lett.*, *36*, L07102, doi:10.1029/2009GL037463.

Parker, E. N. (1957), Sweet's mechanism for merging magnetic fields in conducting fluids, *J. Geophys. Res.*, *62*, 509–520, doi:10.1029/JZ062i004p00509.

Paschmann, G., and P. W. Daly (Eds.) (1998), Analysis methods for multi-spacecraft data, ISSI Sci. Rep. SR-001.

Pollock, C., et al. (2016), Fast plasma investigation for magnetospheric multiscale, *Space Sci. Rev.*, doi:10.1007/s11214-016-0245-4.

Pritchett, P. L., and F. S. Mozer (2009), Asymmetric magnetic reconnection in the presence of a guide field, *J. Geophys. Res.*, *114*, A11210, doi:10.1029/2009JA014343.

Tooley, C. R., R. K. Black, B. P. Robertson, J. M. Stone, S. E. Pope, and G. T. Davis (2015), The Magnetospheric Multiscale constellation, *Space Sci. Rev.*, doi:10.1007/s11214-015-0220-5.

Torbert, R. B., et al. (2014), The FIELDS instrument suite on MMS: Scientific objectives, measurements, and data products, *Space Sci. Rev.*, doi:10.1007/s11214-014-0109-8.

Torbert, R. B., et al. (2015), The electron drift instrument for MMS, *Space Sci. Rev.*, doi:10.1007/s11214-015-0182-7.

Zenitani, S., M. Hesse, A. Klimas, C. Black, and M. Kuznetsova (2011), The inner structure of collisionless magnetic reconnection: The electron-frame dissipation measure and Hall fields, *Phys. Plasmas*, *18*, 122108.